Spatial evolution of multipeaked microwave magnetic envelope solitons in yttrium iron garnet thin films

Mingzhong Wu, Michael A. Kraemer, Mark M. Scott, and Carl E. Patton
Department of Physics, Colorado State University, Fort Collins, Colorado 80523, USA

Boris A. Kalinikos
St. Petersburg Electrotechnical University, 197376 St. Petersburg, Russia
(Received 29 December 2003; published 3 August 2004)

The spatial evolution of multi-peaked microwave magnetic envelope solitons in a thin yttrium iron garnet (YIG) film has been measured and analyzed. The experiments were done on a long and narrow 5-μm-thick single-crystal YIG film strip. Double-peaked and triple-peaked magnetostatic backward volume wave soliton pulses were excited at a nominal carrier frequency of 7.0 GHz. The measurements utilized a movable inductive magnetodynamic probe detection system. The formation of these multi-peaked soliton (MPS) pulses is a two step process. First, an initial single large amplitude pulse gradually separates into two or more nonsolitonic peaks. After a certain propagation time, these nonsolitonic peaks evolve, in sequence, into solitonic peaks with constant phase (CP) and an overall stair-like profile. Typically, the larger amplitude peaks lead in time and become solitonic first. As the MPS signals propagate and decay, the peaks lose their CP character in reverse sequence. The region of existence for the "fully formed" MPS pulses for which all the individual peaks have CP character is extremely narrow, typically on the order of a few tenths of a millimeter. The velocities of the individual peaks scale linearly with the peak powers. A nonlinear response analysis of the peak velocity based on the method of envelopes gives a reasonable match to the data.

DOI: 10.1103/PhysRevB.70.054402 PACS number(s): 75.30.Ds, 76.50.+g, 85.70.Ge

I. INTRODUCTION

Microwave magnetic envelope (MME) solitons were first predicted in 1983 and observed shortly thereafter in yttrium iron garnet (YIG) films.[1,2] Since then, nonlinear MME magnetostatic wave pulses have been the subject of numerous investigations. The MME pulse profiles in magnetic films change significantly with the power of the input microwave pulse signal. (a) For low input powers, one obtains linear MME wave packets that decay and spread out due to the combined effects of damping and dispersion. (b) For moderate input powers, one obtains a single MME soliton pulse. This nonlinear pulse is nondispersive and is formed because of a fine balance between the competing effects of the dispersion and the nonlinear response. (c) For very high input powers, one obtains MME solitons with multiple peaks.

As discussed in Ref. 3, the phase profile of the MME pulse provides a critical signature for solitonic properties. More specifically, Ref. 3 and later papers[4–6] show that single MME soliton pulses have a *constant phase* (CP) profile across the center part of the pulse. It is expected that multi-peaked soliton (MPS) entities should also have peaks with a CP character. Reference 3 has shown that this is indeed the case for solitons with two peaks. Moreover, the data also show that phase jump from one separated peak to the other is 180°.

As a matter of terminology, such a multi-peaked soliton may also be termed a *higher order soliton* (HOS). The node in the first excited state soliton eigenfunction solution to the nonlinear Schrödinger (NLS) equation corresponds a change in sign of the wave function or, equivalently, a phase change of π. In this context, the strict theoretical definition of a higher order soliton relates to specific higher order eigenmode solutions to the NLS equation. As the data below will show, the phase jump between peaks for MPS pulses is generally less than 180°. The distinction between MPS pulses and HOS excitations will be considered below.

References 7 and 8 provide reviews of some of the basic experimental work on multi-peaked soliton signals and modeling based on the Korteweg-de Vries and NLS equations. The early work on water wave systems illustrates the basic properties. Here, an initial wave pulse of sufficiently large amplitude evolves into a soliton with a small number of peaks. The tallest peak is at the front of the evolving wave profile followed by peaks of diminishing intensity behind. As the multi-peaked wave profile propagates, the individual maxima separate from each other. As discussed in Ref. 8, these same types of responses are also found for electrical signals in nonlinear transmission lines.

This work is concerned with the formation and evolution properties of multi-peaked MME soliton pulses. The work builds upon the previous work of Chen *et al.*,[9] Nash *et al.*,[3,10] and Slavin.[11] These authors observed amplitude and phase profiles for MPS signals and obtained useful correlations between the measured power thresholds and HOS theory. These works, however, presented no data on the actual formation, propagation, or decay processes for MPS signals as a function of power or propagation distance. The results presented below demonstrate the complexity and intricacy of MPS formation and propagation.

It was possible to study both double peaked and triple peaked soliton signals. The formation of these MPS waveforms is found to be a two step process in which the initial large amplitude forward propagating pulse first separates into

TABLE I. Yttrium iron garnet (YIG) film parameters.

Parameter	Value
Nominal film thickness d	5.0 μm
YIG Strip width W	2 mm
YIG Strip length L	20 mm
Saturation induction $4\pi M_s$	1750 G
Gyromagnetic ratio γ	-1.76×10^7 rad/Oe s
Ferromagnetic resonance half power linewidth at 5 GHz, ΔH	0.5 Oe

two or more peaks with nonsolitonic character and these peaks then evolve into soliton-type peaks one after another. Once completely formed, the largest amplitude peak typically leads in time and travels faster than the smaller amplitude peak(s). As these MPS signals propagate and decay, the peaks lose their solitonic character, one-by-one.

The organization of this paper is as follows: Section II describes the experiment and provides a summary of key parameters. Section III presents representative data on the spatial evolution and the power dependent peak velocities for the multi-peaked signals. For convenience, the initial conditions and the pulse sequences that yield double peak solitons is given the acronym "MPS2," and "MPS3" is used to label the corresponding conditions and pulse sequences that give triple peak solitons. Section IV provides a nonlinear response analysis based on the classical method of envelopes.

II. SOLITON EXPERIMENT

The experiments utilized a single crystal YIG film 1D excitation structure with time and space resolved detection through an inductive probe arrangement.[12] The film was prepared by standard liquid phase epitaxy techniques on a single crystal gadolinium gallium garnet (GGG) substrate. The nominal thickness was 5 μm. The 5 GHz half power ferromagnetic resonance linewidth was about 0.5 Oe, and spin wave resonance spectra indicated unpinned surface spins.

The measurements were carried out with a long and narrow film strip cut from the YIG wafer. Table I lists the dimensions of the strip and the magnetic parameters of the YIG material. The 10:1 aspect ratio of the strip ensures more-or-less 1D propagation for the excitation and detection structure discussed below. The listed saturation induction $4\pi M_s$ value is the nominal textbook value. The listed gyromagnetic ratio γ corresponds to the free electron value, with $|\gamma|/2\pi=2.8$ GHz/kOe and a Landé g-factor of 2.0.

Figure 1 shows a schematic diagram of the excitation and detection structure. The film is positioned YIG side up, as shown. Input microwave pulse power is applied to the narrow microstrip transducer positioned just above the film and shown somewhat left of center in the diagram. This input produces bi-directional propagating magnetostatic wave (MSW) pulses in the film. The right traveling MSW pulse signal is then detected by the inductive probe. The probe is movable from point to point along the strip, as indicated.

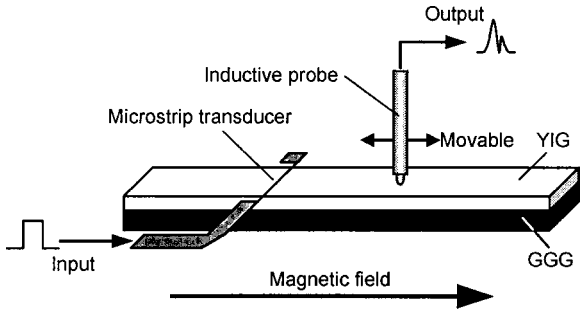

FIG. 1. Schematic diagram of the yttrium iron garnet (YIG) film strip, microstrip transducer for excitation, and movable inductive probe for detection. The YIG strip is supported on a gadolinium gallium garnet (GGG) substrate, as indicated. The microstrip transducer is mounted on the underside of a copper clad substrate, not shown in the diagram. A static magnetic field is applied parallel to the long direction of the YIG strip.

This capability makes it possible to map temporal pulse signals at different spatial positions along the propagation path. The modes propagate in the magnetostatic backward volume wave (MSBVW) configuration with the magnetic field applied parallel to the strip and the signal propagation direction. "Backward" refers to the negative slope of the frequency versus wave number dispersion response for propagation parallel to the field, and the corresponding negative group velocity for the pulses.

For the data given below, the input transducer was positioned about 7 mm from the left end of the film strip. The inductive probe could be positioned at different points on the strip by a two axis stepper motor arrangement, with a resolution of 1 μm. For the data shown below, the transducer to probe distance was varied from 2 to 6 mm, with the probe loop held at the strip center line. The distances from the transducer to the left end of the strip and from the probe to the right end was always about 7 mm or greater. Due to the significant decay in signal amplitude with distance, typically 1.7 dB/mm or so, these large distances eliminated all problems with end reflections.

The probe consisted of a section of 0.5 mm diameter semi-rigid coaxial cable terminated with an inductive loop. The loop was fabricated from a small piece of 50 μm diameter copper wire that was carefully soldered to the center and outer conductors of the open end of the semi-rigid cable. The plane of the inductive loop was oriented perpendicular to the long direction of the film and the static field. The details of the inductive magnetodynamic probe measurement system are given in Ref. 12.

Detailed information on the microwave excitation and detection system, and for MSBVW calibration and characterization procedures, is given in Refs. 9, 12–14. Details that are directly relevant to the MPS2 and MPS3 experiments and analysis are provided below.

Prior to the high power measurements, low power cw and pulse measurements were made to determine the MSBVW band limit frequencies, the group velocity versus frequency response, the frequency versus wave number dispersion characteristics, and suitable operating frequency points for the double and triple peaked pulse measurements. Measurements

TABLE II. Experimental and fitted theoretical parameters for the double peaked (MPS2) and triple peaked (MPS3) pulse signal measurements and analyses.

Parameter	MPS2 regime	MPS3 regime
Nominal applied static field H	1722 Oe	1724 Oe
MSBVW upper cutoff band edge frequency $\omega_B/2\pi$	7.015 GHz	7.022 GHz
Operating point frequency $\omega_k/2\pi$	6.968 GHz	6.984 GHz
Input pulse width T	18 ns	39 ns
Input power P	493 mW	818 mW
Group velocity v_g	2.60×10^6 cm/s	2.74×10^6 cm/s
Dispersion coefficient D	2.61×10^3 rad cm^2/s	Not measured
Fitted applied static magnetic field value H*	1778 Oe	1780 Oe
Fitted film thickness d*	4.9 μm	5.1 μm
Operating point wave number k_0	112 rad/cm	87 rad/cm
Calculated nonlinear coefficient N	-10.7×10^9 rad/s	-10.8×10^9 rad/s

of the propagation time versus distance at low power yielded the group velocities. Further measurements of the group velocity v_g versus frequency ω_k gave the dispersion coefficient $D=\partial^2\omega_k/\partial k^2$, where k is the wave number. The fits of the MSBVW upper cut-off frequencies and the low power group velocities to Damon-Eshbach (DE) theory[15] gave the operating point wave numbers. Note that these fits required small adjustments to the static field as well as the film thickness. The field correction is on the order of the known magnetocrystalline anisotropy fields for YIG materials.

Table II lists key experimental, fitted, and calculated MSW parameters for both sets of measurements. The upper section of the table lists experimental parameters. The middle portion gives parameters based on the DE fits. The last row gives the nonlinear response parameter N, the details for which will be given in Sec. IV. The D and N parameters were evaluated at the indicated MPS2 and MPS3 operating points.

From Table II, the operating point frequencies are 40–50 MHz below the band edge frequencies and the operating point wave numbers are in the 100 rad/cm range. These frequency points are far enough from the band edges to ensure that the power spectrum for the MSW pulses does not extend above the cutoff. At the same time, the operating point wave numbers are still small enough to ensure strong coupling to the 50 μm wide input transducer lines. Note that the value of the applied static magnetic field H controls the position in frequency of the MSBVW band and, in particular, the upper limit frequency of the band. Note also from Table II that the MPS2 and MPS3 H-values and frequency-wave number (ω_k, k_0) operating points are slightly different.

The thresholds for higher order MME soliton formation were studied in detail in Refs. 10 and 11. Generally speaking, MPS formation requires an input pulse with a somewhat higher power and larger width, relative to those for single peaked solitons. The MPS2 and MPS3 solitons were obtained for the input pulse width and power values given in Table II. These choices were based mainly on preliminary observations of the MPS pulses and their evolution with input pulse width and power. Note that the input powers cited above correspond to the actual powers at the microstrip transducer input.

III. FORMATION AND PROPERTIES OF DOUBLE PEAKED AND TRIPLE PEAKED MME SOLITONS

Experimental results on the double peaked and triple peaked solitons are given below. Section III A shows power and phase versus time profiles for selected sequences of propagation distances that demonstrate the formation and decay processes for the MPS2 and MPS3 signals. These processes, while somewhat complicated, demonstrate the specific ways in which the profiles evolve and the phase profiles that accompany these effects. Section III B examines the power dependent velocity responses for the MPS signals.

A. Spatial evolution

Figures 2 and 3 show typical results for the evolution of the MPS2 and MPS3 signals, respectively. Both figures show graphs of the instantaneous power and relative carrier phase as a function of time for different x-displacements of the inductive probe detection point from the input line, as indicated. These detection points range from about $x=2$ mm to $x=6$ mm. These particular detection points have been selected to show, in concert with the chosen input pulse power and width values, the formation and evolution processes for the multi-peaked solitons. Also keep in mind that the leading edge of the pulses occurs on the left side, or for shorter times.

Some of the power versus time profiles in the figures show peaks with small solid circle markers. These markers

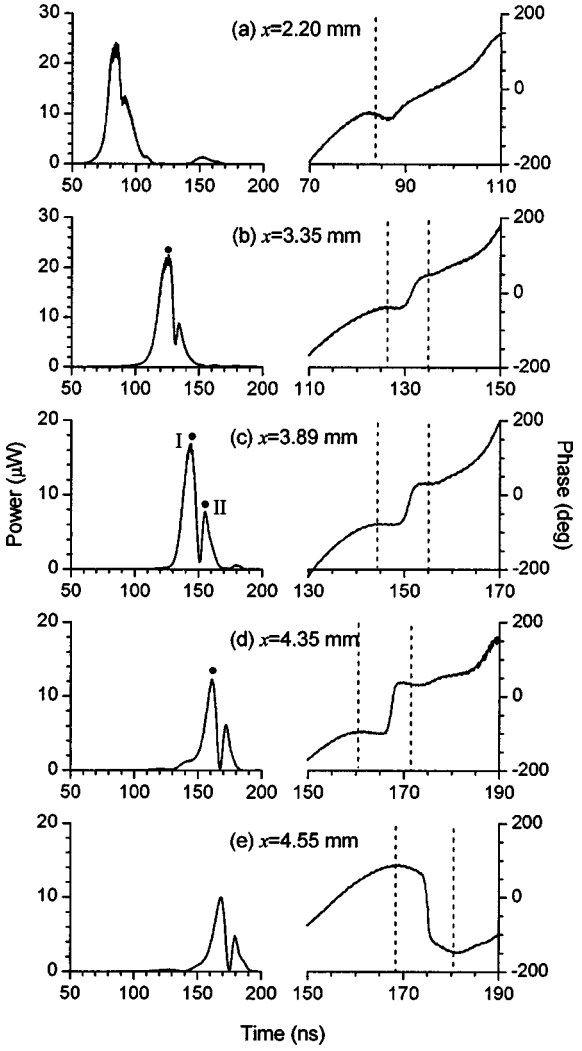

FIG. 2. Representative output power and phase versus time profiles for double peaked pulses. The pairs of graphs are for different inductive probe *x*-positions along the magnetic film strip relative to the input line, as indicated. The nominal static magnetic field along the strip length was 1722 Oe, the carrier frequency was 6.968 GHz, the input pulse width was 18 ns, and the input power to the 50 Ω microstrip line was 493 mW. The solid circle markers on the various peaks in the left side graphs indicate that these peaks have a constant phase solitonic character. In (c), the two solitonic peaks are indexed as I and II. The vertical dashed lines in the right side graphs indicate the positions of the corresponding peaks in the left side graphs.

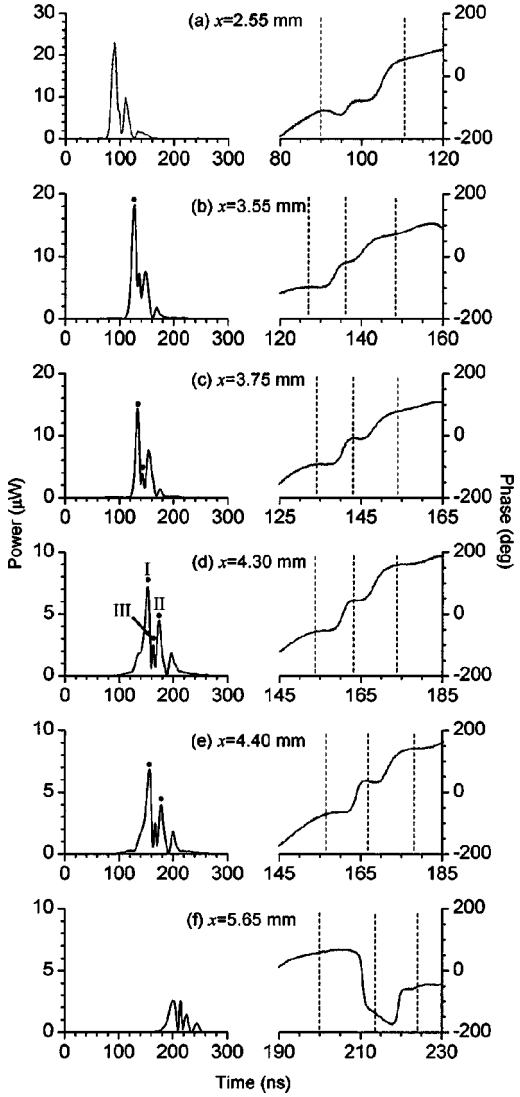

FIG. 3. Representative output power and phase versus time profiles for triple peaked pulses. The pairs of graphs are for different inductive probe *x*-positions along the magnetic film strip relative to the input line, as indicated. The nominal static magnetic field along the strip length was 1724 Oe, the carrier frequency was 6.984 GHz, the input pulse width was 39 ns, and the input power to the 50 Ω microstrip line was 818 mW. The solid circle markers on the various peaks in the left side graphs indicate that these peaks have a constant phase solitonic character. In (d), the three solitonic peaks are indexed as I, II, and III. The vertical dashed lines in the right side graphs indicate the positions of the corresponding peaks from the left side graphs.

serve to identify those peaks with a solitonic character and constant phase across the central peak region. In Figs. 2(c) and 3(d), the main peaks are all solitonic. These have been further labeled as I, II, and III for later reference. The vertical dashed lines shown on the phase versus time graphs show the time positions of the peaks for the power profiles. As a rule, the phase response is relatively flat at the vertical dashed line positions that match solitonic peaks with solid circle markers. In the other cases, the phase response is not so flat.

Both figures show the same MPS evolutionary process. (1) The strongest peak always appears first, or for shorter times; (2) this main peak also develops a CP response early in the spatial evolution; (3) after some distance, weak nonsolitonic peaks develop; (4) after some additional propagation distance, these peaks also develop a CP character; (5) as the propagation continues and the signals decay, the smaller lag peaks lose their CP character first; (6) finally, at long distances, all peaks lose their solitonic character and become dispersive.

The double peaked profiles in Fig. 2 show the above evolutionary process quite clearly. The MPS3 results in Fig. 3 are a bit more complicated. First, there are actually four peaks that appear during the spatial evolution sequence

shown. Second, the small peak that appears third in the development is actually between the first two strong peaks in time, and this third small peak develops a CP profile before the second peak. Finally, note that the fourth and last peak in the sequence stays small and never takes on a CP character.

The power and phase profiles for the complicated and evolving soliton structures in Figs. 2 and 3 mirror and extend previous results for single peaked solitons.[3–6] These studies have shown that, when there is appropriate compensation between the dispersion and the nonlinear response, one can form a robust and non-dispersive bright MME soliton with a CP profile across the peak. Constant phase, therefore, provides a simple unambiguous criterion for bright MME soliton formation.

The key result from Figs. 2 and 3 is that this CP criterion carries over from single peaked solitons to the MPS case. From Fig. 2, for example, one can see that the main peak first takes on a CP character, as in Fig. 2(b). At the point where the MPS2 formation is complete, as in Fig. 2(c), the secondary peak has also taken this CP character. Then, as the soliton decays, the secondary peak is the first one to lose this character, as in Fig. 2(d). In Fig. 2(e), the main peak has also lost its CP character and the MPS2 pulse has completely decayed back to a non-solitonic double peaked signal.

Figure 3 shows the same trend, but with some small differences. The small third peak that is first in evidence in Fig. 3(b) is actually the second peak to take on a CP character, as in Fig. 3(c). In contrast, the second peak to form, already in evidence in Fig. 3(a), takes on a CP character in Fig. 3(d). The loss of CP character upon decay does follow the expected trend, with the weakest peak changing first, as in Fig. 3(e) followed by the largest secondary peak in Fig. 3(f).

Considered as a whole, the above data demonstrate, among other things, the ambiguous nature of the multi-peaked soliton concept from an experimental point of view. One might, for example, define a double peaked soliton as a pulse profile with two peaks, both of which have CP character. The current data show, however, that such a profile only occurs over a relatively small range of propagation distances. For the particular situation in Fig. 2, detailed measurements for a much finer increment in probe position show that the MPS2 existence region spans a distance of only about 0.4 mm or so. For the MPS3 response in Fig. 3, this existence region is even shorter.

Comments are also appropriate here on the connection between well known and extensively discussed higher order soliton (HOS) eigenmode solutions to the NLS equation[8,16,17] and the experimental multi-peaked soliton signals examined here. Analytic and numerical solutions to the NLS equation demonstrate both the simple eigenmode physics and the complexity of these entities. At the basic level, these higher order eigenmodes have nodes that correspond to a phase change in π from peak to peak. Such a change was demonstrated experimentally in Fig. 7(d) of Ref. 3. The complexity of these HOS eigenmodes is made clear from the breathing properties of the modes and the periodic evolution between wave forms with different shapes and different numbers of peaks shown in Refs. 7, 8, 16, and 17.

The data presented in Figs. 2 and 3 make it clear that the experimental situation for higher order MME solitons is even more complicated than one might expect from the eigenmode solutions to the NLS equation. For bonafide eigenmodes, one expects to see a π phase jump associated with each node in the soliton envelope function. The data in Figs. 2 and 3 show jumps, but these are different from π. The π jump in Fig. 7(d) of Ref. 3 occurs for well separated peaks. The solitonic peaks in Figs. 2(c) and 3(d) above are not separated at all. In cases where the MPS signal can evolve to a limit of well separated solitonic peaks, it may well be that the phase jumps move to π values. However, the data show that the multi-peaked solitons decay into nonsolitonic entities before this can happen. The books cited above discuss amplitude profiles for HOS signals, but generally make no comments about phase. This is a ripe subject for further study, both experimentally and theoretically.

One can see from the time and distance scales in Figs. 2 and 3 that the pulse velocities are on the order of 3×10^6 cm/*s*. Such velocities are about the same as for single soliton pulses. A full analysis of the MPS data show, however, that the individual peaks have different velocities that scale with amplitude. This new feature is considered below.

B. Power dependent peak velocities

Work by Xia *et al.*[18] has shown that the average velocity of MME soliton wave packets is, in general, power dependent, and one would expect that these individual peak velocities should also change with amplitude. In order to examine these responses experimentally, peak position versus time data were obtained for the two solitonic peaks indicated in Fig. 2(c) and the three corresponding peaks in Fig. 3(d). These data were obtained over the full range of *x*-positions for which all of the peaks remain solitonic, as defined by the CP condition. As noted above, the range in *x*-values for such a full solitonic response was small, about 0.4 mm for the MPS2 case and only 0.1 mm for the MPS3 data.

Figure 4 shows the results of these measurements. Figure 4(a) is for the MPS2 signals. These data extend from $x = 3.69$ mm to $x = 4.09$ mm, the range that matches in Fig. 2(c). The labels I and II correspond to the same labels used for the peaks in Fig. 2(c). Figure 2(b) is for the MPS3 signals. These data extend from $x = 4.23$ mm to $x = 4.35$ mm, the range that matches in Fig. 3(d). The labels I, III, and II are for the main peak, the weak middle peak, and the stronger lag peak identified in Fig. 3(d) profile. The solid lines in both graphs represent linear best fits to the data.

The data and fits in Fig. 4 show that the solitonic peak displacements are all linear in time and give velocities in the 3×10^6 cm/s range. By careful inspection, however, one can also see that there are small changes in the peak velocities as one goes from peak to peak. The actual fits show, for example, that the peak I velocity in Fig. 4(a) is about 5% greater than the peak II velocity. For Fig. 4(b), the peak I velocity is about 7% greater than the peak III velocity. These increases, moreover, correlate with the peak amplitudes.

Figure 5 shows the velocities and standard errors from the fitted slopes of the lines in Fig. 4 for the different peaks. The solid circle points in Fig. 5(a) and 5(b) show these velocities plotted against the corresponding peak powers from the

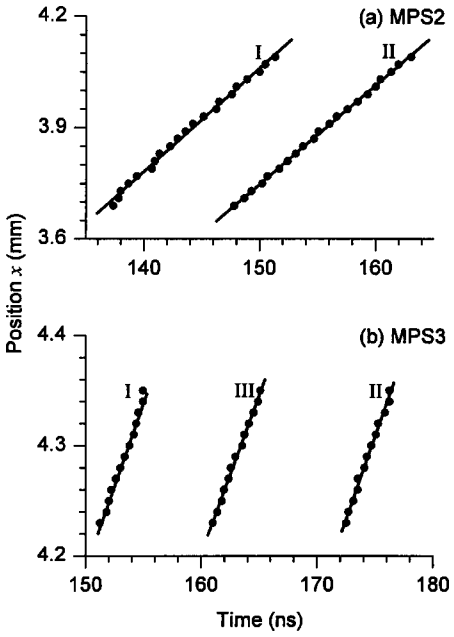

FIG. 4. Graphs (a) and (b) show position x versus time for the I and II MPS2 peaks in Fig. 2(c) and the I, II, and III MPS3 peaks in Fig. 3(d), respectively. The data correspond to the ranges of distances for which all of the peaks were solitonic. The solid lines indicate linear best fits to the data.

graphs in Figs. 2(c) and 3(d), respectively. The Roman numeral indices correspond to those in Figs. 2–4. The data points at zero power indicate the measured group velocities for the pulse signals at low power. The solid lines indicate linear fits to the data. Note that the low power velocities for the MPS2 and MPS3 configurations are slightly different. This is because of the slightly different operating points.

Three important results are evident from Fig. 5. First, the data show that all of the solitonic peaks travel faster than the low power pulse signals. Second, it is clear that each peak travels with its own distinct velocity. Third, one can see that the change in velocity with power is roughly linear in each case. From Fig. 5(a), the MPS2 peak velocity increases with power at a rate of about 1.4×10^4 cm/(s$\cdot\mu$W). From Fig. 5(b), the corresponding MPS3 change is about 4.5×10^4 cm/(s$\cdot\mu$W). These increases in peak velocity with power are not unexpected. In Ref. 18, Xia *et al.* provided data on the average MPS velocity and showed that this velocity increases with power. The current results extend these previous results to show that the *individual peaks that make up the multi-peaked solitons* also move with power dependent velocities. Note also that one finds similar responses for multi-peaked surface water wave solitons and electromagnetic wave solitons in nonlinear transmission lines.[7,8] These power dependent soliton peak velocities are a direct effect of the nonlinear interactions that drive the soliton formation in the first place.

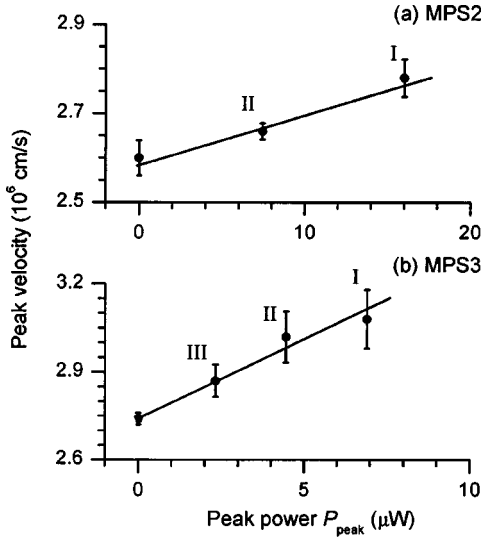

FIG. 5. Graphs (a) and (b) show velocities and standard errors from the fitted slopes of the lines in Fig. 4 as a function of the peak power P_{peak} for the indicated MPS2 and MPS3 peaks. The data points at $P_{peak}=0$ show group velocities for the corresponding low power MSW signals. The solid lines indicate linear fits to the data.

These new data expand significantly on the results of Ref. 18. Those data showed that the averaged soliton center point travels with an average velocity between launch and detection antennas that *increases* with the input pulse peak power, and that there are distinct *plateaus* in this velocity response at *discrete* velocity values. Based on connections with modulational instability considerations, Ref. 18 also presented a simple theoretical connection between MME soliton velocity and soliton order. Note, however, that the Ref. 18 measurements were based on time of flight between widely spaced antenna elements, and not the small increment instantaneous position versus time determinations used here.

The entirely local, rather than averaged velocity results obtained here show quite clearly that the velocity of the individual peaks for multi-peaked solitons also scales with the peak power. The scaling applies to both double peaked and triple peaked solitons. This velocity response is related to the nonlinear shift in the MSW dispersion curve with power. Section IV will give a simple but quantitative analysis of the power dependent velocity for nonlinear MSW signals that makes a direct connection with the data given above.

The power dependent MPS peak velocity, now quantified, provides an easy explanation for the evolution of the peaks with propagation distance shown in Figs. 2 and 3. The fact that the higher peaks travel faster causes the individual MPS peaks to move apart as the average propagation distance increases. This gradual separation is clearly evident in both figures. In Fig. 2, for example, as one moves from Figs. 2(b) and 2(d) in sequence, MPS2 peaks I and II become more and more separated. In Fig. 3, a close examination shows that MPS3 peaks I and III overlap somewhat in Fig. 3(c) and become more separated in Figs. 3(d) and 3(e).

IV. THEORETICAL CONNECTIONS

The above data reveal a number of previously unrealized features of multi-peaked solitons. The individual peaks that make up a MPS waveform, for example, form and take on their individual CP characters in sequence, and then lose the same CP character in reverse sequence. The spatial interval over which all of the peaks maintain the CP character taken

to define a soliton in the first place is rather narrow. For the data presented above for MPS2 and MPS3 signals, these existence regions amounted to only a few tenths of a millimeter of the overall propagation path. The individual peaks, moreover, exhibit power dependent velocities.

The purpose of this section is to provide some brief connections between the above effects and soliton theory. Work is in progress on a full theoretical analysis of the MPS response based on the NLS equation. The discussion below provides (a) qualitative considerations on MPS peak formation times and lifetimes, and (b) a simple quantitative analysis of peak velocity.

The formation of envelope solitons in general occurs as a result of a nonlinear phase shift at large amplitude that compensates for the usual dispersive phase shift that causes the wave packet to spread out and lose amplitude. Two analyses of soliton formation times based on numerical solutions to the NLS equation have been reported recently. For the case without dissipation, Staudinger *et al.* defines a soliton formation time T_s as the time after launch when the amplitude of the propagating pulse stops changing and holds constant.[19] For the more realistic case with dissipation included, Slavin and Benner define T_s as the time at which the amplitude decay rate becomes equal to twice the linear decay rate.[20] This definition is based on the theoretical solution to the NLS equation with small damping. In this limit of small damping, the NLS analysis gives an amplitude decay rate of twice the linear decay rate.

Both of the above references consider only the formation of single, or order one, solitons. Both approaches give a soliton formation time that is on the order of the well established nonlinear response time

$$T_N = \frac{\pi}{|N||u|^2}. \tag{1}$$

The nonlinear response parameter N gives the change in the MSW frequency with the MSW power and may be written as $N = \partial\omega_k/\partial|u|^2$, where $\omega_k(k,|u|)$ is the power dependent MSW frequency for a specific wave number k, and $|u|^2$ represents the MSW power. As used below for the analysis of the power dependent soliton velocity, the parameter u is a scalar complex amplitude defined through $u = m/(2^{1/2}M_s)$, where m is the rms dynamic magnetization and M_s is the saturation magnetization of the material. The frequency $\omega_k(k,|u|)$ may be obtained operationally by replacing the $4\pi M_s$ terms in the DE MSBVW dispersion relation with $4\pi M_s(1-|u|^2)$. The $\partial\omega_k/\partial|u|^2$ derivative is evaluated at the operating point wave number k_0 and frequency ω_0, and at $|u|=0$. The corresponding MPS2 and MPS3 N-values are shown in Table II.

Equation (1) has a simple physical interpretation as the time for a cw signal of amplitude $|u|$ to experience a nonlinear phase change of π radians. The connection with the soliton formation time is also clear. A large amplitude peak will have a *shorter* nonlinear response time than a small peak and, hence, will acquire soliton characteristics earlier. While the work in Refs. 19 and 20 and applies this connection to single solitons, by simple extension, one may also apply this principle to the individual peaks for MPS pulses.

In light of the above nonlinear phase shift considerations and the data of the previous section, it is reasonable to consider the formation of multi-peaked solitons as a two step process. In the first step, a single pulse of sufficient amplitude breaks into one or more nonsolitonic peaks. In the second step, these nonsolitonic peaks evolve into solitonic peaks in sequence, based on their starting amplitudes.

In terms of this two step process, the MPS2 data in Fig. 2 indicate that step one occurs over a span of x-distances from the launch antenna of 0–3.35 mm. This is followed by the sequential solitonic peak formation processes for the two peaks from about 3.35 mm to 3.89 mm. The MPS3 data in Fig. 3 indicate a step one process over a distance from $x=0$ to $x \approx 3.55$ mm and a step two process for $x \approx 3.55-4.3$ mm. The fact that the weaker MPS3 peak III achieves a CP character before the stronger MPS3 peak II is attributed to its proximity to the very strong MPS3 peak I and a possible phase dragging response.

Consider now the lifetime of the CP peaks in the MPS2 and MPS3 experiments. In line with the above formation time argument in which T_s scales with T_N, and hence with the initial amplitude, one may also argue that the lifetime of the solitonic peaks, once formed, should also scale with the peak amplitude. This argument is supported by the established condition for soliton formation. Slavin and Benner write this condition as[20]

$$|N|u_{\text{th}}{}^2 = \frac{1}{4}|D|\left[\frac{(2n-1)\pi}{|v_g|T_{\text{in}}}\right]^2, \tag{2}$$

where u_{th} is the amplitude of the initial dynamic magnetization pulse at input, in reduced u-units defined above, and v_g and T_{in} are the low power group velocity and temporal width of the MSW input pulse, respectively. The parameter n denotes the soliton order. The above is subject to the additional constraint imposed by the Lighthill criterion, $ND<0$. These considerations are reviewed in Ref. 21.

Equation (2) gives the threshold amplitude u_{th} for a square input pulse of width T_{in} in order to form a soliton of order n at some later time. The actual input amplitude u_{in} must be *greater* than u_{th} for the soliton to form in a finite time. Just as the formation time will decrease as $(u_{\text{in}}-u_{\text{th}})$. increases, it stands to reason that the lifetime of this soliton, once formed, will also scale with $(u_{\text{in}}-u_{\text{th}})$. The observation from the experiments that the larger peaks maintain their solitonic character longer and the smaller peaks lose their CP character quicker is consistent with the above. One cannot, of course, use Eq. (2) to obtain threshold amplitudes for individual MPS peaks. This expression only applies to pure HOS nonlinear eigenmodes. Further numerical analysis is underway to model these systems and elucidate the MPS peak formation times and lifetimes.

Turn now to the MPS peak velocities. The data in Figs. 4 and 5 show that the MPS2 and MPS3 peaks have velocities that scale linearly with the peak power and extrapolate to the measured group velocities in the low power limit. The method of envelopes that forms the basis of the NLS equation model can be used to model this response and give velocities that are in the same range as the data above. The

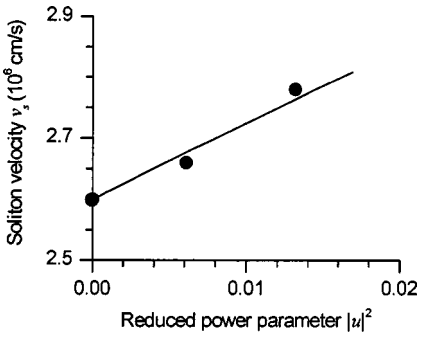

FIG. 6. Soliton velocity versus the reduced power parameter $|u|^2$. The solid line shows the computed result from Eq. (5) for applicable MPS2 parameters. The solid points show the MPS2 data points from Fig. 5(a), based on a $|u|^2$ to peak power calibration factor of 8.2×10^{-4} μW^{-1}.

calculation and results for MPS2 parameters are given below.

The first step in the method of envelopes NLS analysis involves a series expansion of the frequency ω_k of a cw signal that takes the form[21]

$$\omega_k = \omega_0 + v_g(k-k_0) + \tfrac{1}{2}D(k-k_0)^2 + N|u|^2, \tag{3}$$

where ω_0 and k_0 denote the operating point frequency and wave number parameters, respectively, and $|u|$ represents the carrier amplitude. Differentiation with respect to k leads to a power dependent group velocity that may be identified with the soliton velocity v_s,

$$v_s = v_g + D(k-k_0) + \frac{\partial N}{\partial k}|u|^2. \tag{4}$$

The $(k-k_0)$ factor is obtained from Eq. (3) and the condition $\omega_k=\omega_0$. Nash *et al.*[3] have shown that the CP condition for solitons corresponds to a zero frequency shift as well. One then obtains a relatively simple expression for the soliton velocity,

$$v_s = \sqrt{v_g^2 - 2DN|u|^2} + \frac{\partial N}{\partial k}|u|^2. \tag{5}$$

From a straightforward analysis based on the nonlinear dispersion $\omega_k(k,|u|^2)$ response, the second term on the right side of Eq. (5) is less than 2% of the square root term over the range of v_s and u-values applicable in the experiment, and can be neglected. Moreover, the positive $-2DN|u|^2$ term inside the square root is also small enough to give a *nearly linear* v_s versus $|u|^2$ response over the range of v_s values that match experiment.

Figure 6 shows a plot of the soliton velocity v_s as a function of $|u|^2$ based on the above analysis with the second term on the right hand side of Eq. (5) neglected. The plot was obtained for the MPS2 parameters in Table II. The 0–0.02 range for the horizontal axis was selected to give v_s values that match the same range of values as in Fig. 5(a). The solid points in the figure are transferred from Fig. 5(a), based on an *ad hoc* $|u|^2/P_{\text{peak}}$ ratio of 8.2×10^{-4} μW^{-1}. Based on this ratio, one obtains $|u|$ values for the MPS2 peaks I and II of about 0.11 and 0.08, respectively. These values are right at the high end of the 0.01–0.10 range that is typical for MME solitons.[14] The $|u|$ values for multi-peaked solitons should be at the high end of this range, of course, because the higher powers are needed to produce MPS pulses in the first place.

In closing this velocity discussion, it is useful to consider the implications of these peak velocity results for average velocities. In Ref. 18, averaged center of mass velocities were obtained from amplitude weighted positions in time at specific x-positions. For multi-peaked solitons, this same average velocity can be approximated from a weighted average of the individual peak velocities according to

$$v_{\text{av}} = \sum_{i=1}^{n}\left(\frac{|u_i|}{\sum_{i=1}^{n}|u_i|}\right)v_i. \tag{6}$$

The $|u_i|$ and v_i denote the peak amplitudes and velocities of the individual MPS peaks and the sum is over the number of peaks present, typically the same as the soliton order n.

Based on the definition in Eq. (6), the data and analyses above can be used to obtain v_{av} values for the MPS2 and MPS3 soliton profiles shown in Figs. 2 and 3. In the MPS2 case, one obtains $v_{\text{av}}=2.71\times10^6$ cm/s, which is about 4.2% higher than the corresponding low power group velocity v_g. For the MPS3 case, one obtains $v_{\text{av}}=2.98\times10^6$ cm/s, which is about 8.8% higher than the corresponding v_g. These simple evaluations show the basis of the empirical conclusion obtained in Ref. 18 from rather tedious weighted averages over complicated profiles. These results show that the increase in the average soliton velocity with soliton order is a direct result of the peak power dependent velocities of the individual peaks and the increase in the weighted average of these velocities with soliton order.

V. SUMMARY AND CONCLUSION

The spatial formation and propagation properties of double peaked and triple peaked MME solitons have been studied experimentally. The formation of a multi-peaked MME soliton takes place in two steps. First, the initial large amplitude forward propagating pulse gradually breaks into two or more separate but non-solitonic peaks. After some propagation time, these non-solitonic peaks evolve into soliton-type peaks in sequence. Typically, the larger amplitude peaks become solitonic first. A completely formed multi-peaked soliton is taken to occur when all of the peaks have attained a CP profile across the central portion of the peak region. The largest amplitude peak is usually ahead of and travels faster than the smaller amplitude peaks. As the MPS signals propagate and decay, the peaks lose their solitonic character one-by-one and revert into nonsolitonic peaks, typically in reverse sequence.

The data indicate that the individual MPS peak formation is faster and the lifetime of the solitonic peak is longer for a higher amplitude. This can be qualitatively explained in terms of the amplitude driven nonlinear response time. The higher the amplitude, the more rapid the nonlinear frequency shift. A model for the power dependent soliton peak velocity was developed, based on the method of envelopes frequency expansion approach. The model gives good agreement with experiment.

ACKNOWLEDGMENTS

This work was supported in part by the National Science Foundation, Grant No. DMR-0108797, the U. S. Army Research Office, Grant No. DAAD19-02-1-0197, and the North Atlantic Treaty Organization, Grant PST/CLG 980077. The films used in this work were provided by Professor Yuri K. Fetisov, Moscow Institute of Radio Engineering, Electronics, and Automation (MIREA), Moscow, Russia. The authors are also grateful to Professor Yuri S. Kivshar, Australian National University, Canberra, Australia for helpful discussions.

[1] A. K. Zvezdin and A. F. Popkov, Zh. Eksp. Teor. Fiz. **84**, 606 (1983) [Sov. Phys. JETP **57**, 350 (1983)].
[2] B. A. Kalinikos, N. G. Kovshikov, and A. N. Slavin, Pis'ma Zh. Eksp. Teor. Fiz. **38**, 343 (1983) [Sov. Phys. JETP **38**, 413 (1983)].
[3] J. M. Nash, P. Kabos, R. Staudinger, and C. E. Patton, J. Appl. Phys. **83**, 2689 (1998).
[4] B. A. Kalinikos, N. G. Kovshikov, and C. E. Patton, Phys. Rev. Lett. **78**, 2827 (1997).
[5] P. A. Kolodin, P. Kabos, C. E. Patton, B. A. Kalinikos, N. G. Kovshikov, and M. P. Kostylev, Phys. Rev. Lett. **80**, 1976 (1998).
[6] B. A. Kalinikos, N. G. Kovshikov, and C. E. Patton, Appl. Phys. Lett. **75**, 265 (1999).
[7] P. G. Drazin and R. S. Johnson, *Solitons: an introduction* (Cambridge University Press, Cambridge, 1989).
[8] M. Remoissenet, *Waves Called Solitons: Concepts and Experiments* (Springer, Berlin, 1999).
[9] M. Chen, M. A. Tsankov, J. M. Nash, and C. E. Patton, Phys. Rev. B **49**, 12 773 (1994).
[10] J. M. Nash, C. E. Patton, and P. Kabos, Phys. Rev. B **51**, 15 079 (1995).
[11] A. N. Slavin, Phys. Rev. Lett. **77**, 4644 (1996).
[12] M. M. Scott, Ph.D. thesis, Department of Physics, Colorado State University, 2002.
[13] N. G. Kovshikov, B. A. Kalinikos, C. E. Patton, E. S. Wright, and J. M. Nash, Phys. Rev. B **54**, 15 210 (1996).
[14] H. Y. Zhang, P. Kabos, H. Xia, R. A. Staudinger, P. A. Kolodin, and C. E. Patton, J. Appl. Phys. **84**, 3776 (1998).
[15] D. D. Stancil, *Theory of Magnetostatic Waves* (Springer-Verlag, New York, 1993), p.109.
[16] Y. S. Kivshar and G. P. Agrawal, *Optical Solitons* (Academic Press, San Diego, 2003).
[17] G. P. Agrawal, *Nonlinear Fiber Optics* (Academic Press, San Diego, 1995).
[18] H. Xia, P. Kabos, R. A. Staudinger, C. E. Patton, and A. N. Slavin, Phys. Rev. B **58**, 2708 (1998).
[19] R. A. Staudinger, P. Kabos, H. Xia, B. T. Faber, and C. E. Patton, IEEE Trans. Magn. **34**, 2334 (1998).
[20] A. N. Slavin and H. Benner, Phys. Rev. B **67**, 174421 (2003).
[21] A. N. Slavin, B. A. Kalinikos, and N. G. Kovshikov, in *Nonlinear Phenomena and Chaos in Magnetic Materials*, edited by P. E. Wigen (World Scientific, Singapore, 1994), Chap. 9.